arXiv:2507.00583v4 [cs.CV] 3 Feb 2026

AI-Generated Video Detection via Perceptual Straightening

Christian Internò[1,3*] **Robert Geirhos**[2] **Markus Olhofer**[3] **Sunny Liu**[4]
Barbara Hammer[1] **David Klindt**[4]
[1] Bielefeld University [2] Google DeepMind
[3]Honda Research Institute EU [4]Cold Spring Harbor Laboratory

Abstract

The rapid advancement of generative AI enables highly realistic synthetic videos, posing significant challenges for content authentication and raising urgent concerns about misuse. Existing detection methods often struggle with generalization and capturing subtle temporal inconsistencies. We propose ***ReStraV***(Representation Straightening for Video), a novel approach to distinguish natural from AI-generated videos. Inspired by the *"perceptual straightening"* hypothesis [1, 2]—which suggests real-world video trajectories become more straight in neural representation domain—we analyze deviations from this expected geometric property. Using a pre-trained self-supervised vision transformer (DINOv2), we quantify the temporal curvature and stepwise distance in the model's representation domain. We aggregate statistics of these measures for each video and train a classifier. Our analysis shows that AI-generated videos exhibit significantly different curvature and distance patterns compared to real videos. A lightweight classifier achieves state-of-the-art detection performance (e.g., 97.17% accuracy and 98.63% AUROC on the VidProM benchmark [3]), substantially outperforming existing image- and video-based methods. *ReStraV* is computationally efficient, offering a low-cost and effective detection solution. This work provides new insights into using neural representation geometry for AI-generated video detection.

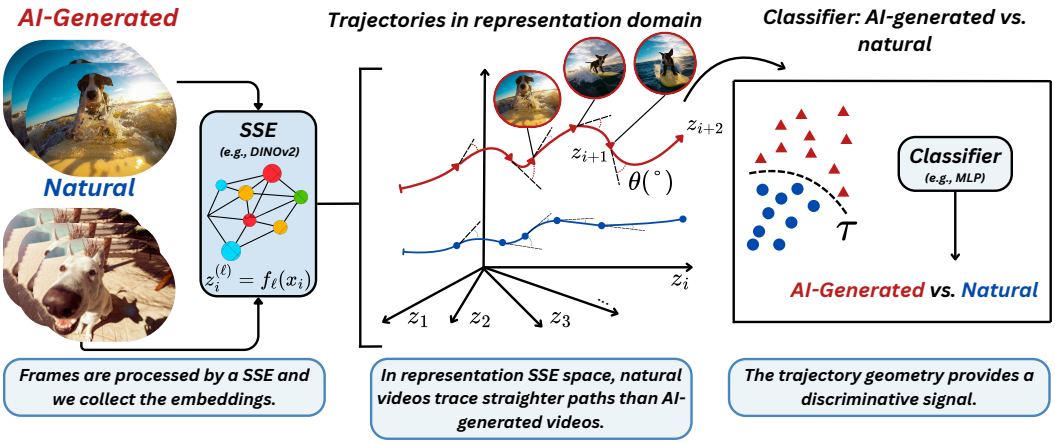

Figure 1: **The ReStraV method for AI-video detection.** Inspired by "perceptual straightening," our approach leverages the geometric insight that natural videos form "straighter" feature trajectories (z_i) than generated ones. The temporal curvature (Eq. 1) serves as the discriminative signal for detection.

*Correspondence to: christian.interno@uni-bielefeld.de
Code: https://github.com/ChristianInterno/ReStraV

1 Introduction

Generative AI has significantly advanced in synthesizing realistic video content [4–6]. Early approaches (e.g., generative adversarial networks, variational autoencoders) struggled with fidelity and temporal coherence [7–9]. However, rapidly evolving large-scale foundation models have introduced sophisticated generative techniques [10, 11]. These methods, often diffusion models [12] and transformer-based architectures [13, 14], can produce near-photorealistic videos from text or initial frames. As these systems improve, the ability to easily generate convincing synthetic videos raises pressing concerns about malicious manipulation and fabricated visual media [15].

Robust strategies to detect AI-generated content are therefore urgently needed [6, 11, 16]. Detecting AI videos is more challenging than AI generated image due to temporal consistency requirements that necessitate thorough analysis across frames [3, 17]. Traditional deepfake detectors, often tuned to specific artifacts (e.g., face-swapping irregularities), may not generalize to diverse generative methods [18]. Moreover, large-scale pretrained foundation encoders may not explicitly learn features optimized for AI content detection. Watermarking is one option but relies on model operators' goodwill and can be circumvented [19–22]. Thus, detection methods are needed that capture AI generation anomalies, regardless of the underlying generative approach.

This work explores neural representational distance and curvature (formally defined in Eq. (1)) as discriminative signals for fake video detection. An overview of *ReStraV* is provided in Fig. 1. According to the *perceptual straightening hypothesis*, natural inputs map to straight paths in neural representations while unnatural sequences form curved trajectories [1, 2]. This has been verified in neuroscience, psychophysics, on CNNs and LLMs [1, 23]. It is motivated by the idea that predictive coding might favor straight temporal trajectories in latent space because they are more predictable.

Taking inspiration, in this work, we hypothesize a distinction between natural and AI generated videos in artificial neural networks (ANNs). While ANNs may not perfectly replicate biological straightening [1, 2, 24], we expect their learned representations to show AI-generated videos as more curved in activation space than real videos. We surmise synthetic videos exhibit curvature patterns deviating from the lower curvature trajectories of real events, supported by differing ANN representational dynamics for natural versus artificial videos [24], as illustrated in Fig. 2A and Fig. 4.

To test this hypothesis, we use the DINOv2 ViT-S/14 pretrained visual encoder [25], chosen for its sensitivity to generative artifacts (Fig. 2B). For each video, we extract frame-level complete set of patch embeddings and Classify token (CLS) from DINOv2's final transformer block (`block.11`). From this trajectory, we quantify local curvature (angle between successive displacement vectors, measuring path bending) and stepwise distance (change magnitude between consecutive frame representations), as in Eq. (1). We then derive descriptive statistics (mean, variance, min, max; examples in Fig. 5) from these per-video time series of curvature and distance. These aggregated geometric features (Section 5) are used by a lightweight classifier (Section 6) to distinguish real from AI content.

ReStraV re-purposes DINOv2 as a "feature space" for temporal anomalies. DINOv2's extensive training on natural data provides a latent space where real video trajectories should be characteristically smooth or "straight" (Fig. 2A, Fig. 4). Deviations, like increased jitter or erratic curvature often in AI videos, become discernible geometric signals of synthetic origin. Importantly, *ReStraV* is computationally efficient, processing videos in approximately 48 ms end-to-end (including DINOv2 forward pass). *ReStraV* is thus a low-cost alternative to resource-intensive methods (details in Section 6). By exploiting ANN's activation dynamics, *ReStraV* offers a simple, interpretable AI-video detection approach (experimental validation in Section 7). Our contributions are as follows:

1. We propose a novel, simple, cost-efficient, and fast representational geometry strategy for AI-generated video detection, leveraging neural activation distance and curvature as reliable indicators of generated videos.
2. We show the approach yields a reliable "fake video" signal across vision encoders, even those not trained on video data; DINOv2's [25] self-supervised representations excel without task-specific tuning.
3. We demonstrate through extensive experiments on diverse benchmarks (VidProM [3], GenVidBench [17], and Physics-IQ [26]) and models, that *ReStraV* improve detection accuracy that often surpasses state-of-the-art (SoTA) methods.

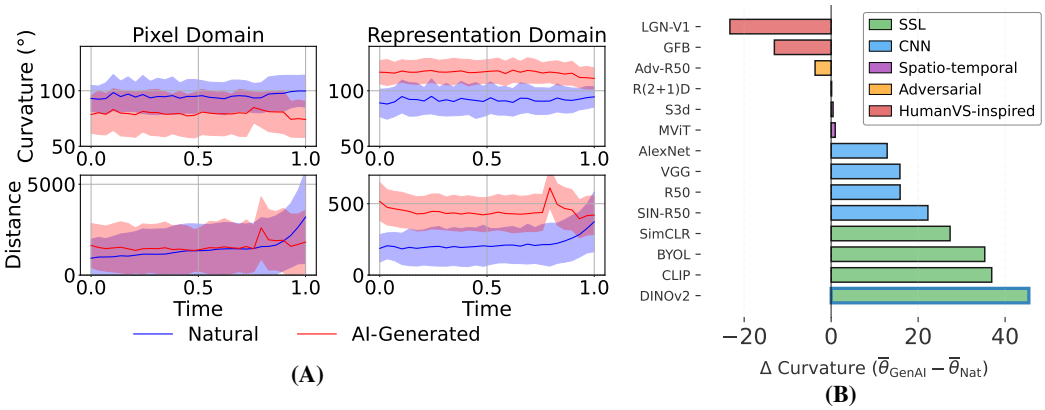

Figure 2: **(A)** In pixel space (left), video trajectory metrics (curvature, distance; see Eq. (1) for details) between natural vs. AI-generated videos show substantial overlap. In contrast, DINOv2 representations (right) straighten natural trajectories, clearly separating natural and AI-generated videos. **(B)** The mean curvature gap ($\Delta\theta$) between AI-generated and natural videos across various visual encoders. HVS-inspired models (red) exhibit negative deltas, straightening both natural and AI videos equally, while SSL models (green), particularly DINOv2, show the largest positive deltas.

2 Related work: detecting AI–generated videos

Detecting AI-generated video (see Section A for an AI generative models overview) is becoming increasingly challenging. Many early detection efforts, including image-based detectors (CNNSpot [27], Fusing [28], Gram-Net [16], FreDect [29], GIA [30], LNP [31], DFD [32], UnivFD [33]), focused on spatial or frequency-domain artifacts within individual frames. However, their frame-centric nature limits their efficacy on videos, where temporal consistency is paramount.

Dedicated video detectors, such as adapted action recognition models (TSM [34], I3D [35], SlowFast [36]) and Transformer-based (X3D [37], MVIT-V2 [38], VideoSwin [39], TPN [40], UniFormerV2 [41], TimeSformer [42], DeMamba [43], aim to learn motion anomalies and temporal inconsistencies. While advancing temporal modeling, they require extensive training and may still struggle across rapidly evolving AI generative models. Those approaches may overlook a more fundamental signal: geometric distortions in the temporal trajectory of neural representations. We hypothesize that the geometric properties of these trajectories—reflecting the inherent smoothness and predictability of natural dynamics that generative models fail to replicate—offer a more robust signal for detection. Unlike related work in video quality assessment that also uses trajectories [44, 45], our focus is distinctly on detecting synthetic content, regardless of its perceptual quality.

3 Perceptual straightening definition

Natural input sequences are often highly complex. For instance, even a video of a simple object moving across an image will be a nontrivial sequence of points traveling through a high dimensional pixel space. Specifically, this sequence will be curved since the only straight video is an interpolation between two frames. According to the temporal straightening hypothesis, biological visual systems simplify the processing of dynamic stimuli by transforming curved temporal trajectories into straightened trajectories of internal representations [1, 2]. Although the raw pixel trajectories of natural videos are highly curved, the neural representations in the human visual system become straightened to support efficient temporal prediction and processing[2]. In this article, we exploit this property to detect differences between AI-generated and natural videos.

Formally, let a video segment be represented by a temporal sequence of T feature vectors, $\mathcal{Z} = (z_1, z_2, \ldots, z_T)$, where each $z_i \in \mathbb{R}^D$ is the embedding for the i-th sampled frame (with i being the frame index). The displacement vector between consecutive frame representations is defined as $\Delta z_i = z_{i+1} - z_i$, for $i = 1, \ldots, T-1$. The magnitude of this displacement, which we term the stepwise distance, is $d_i = \|\Delta z_i\|_2$. Following [1, 2], the curvature θ_i of the representation trajectory is defined as the angle between successive displacement vectors, Δz_i and Δz_{i+1}:

$$\theta_i = \overbrace{\arccos\Big[\underbrace{\frac{\overbrace{\Delta z_i}^{\text{Consecutive Displacement}} \cdot \overbrace{\Delta z_{i+1}}^{\text{Consecutive Displacement}}}{\underbrace{\|\Delta z_i\|_2}_{\text{Temporal Distance } (d_i)} \; \underbrace{\|\Delta z_{i+1}\|_2}_{\text{Temporal Distance } (d_{i+1})}}}_{\text{Cosine similarity between } \Delta z_i \text{ and } \Delta z_{i+1}}\Big]}^{\text{Curvature}}, \quad (1)$$

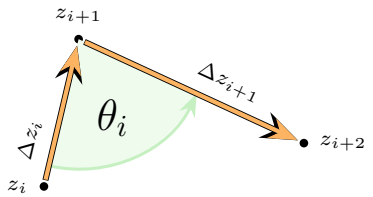

Figure 3: Trajectory curvature Eq. (1).

$i = 1, \ldots, T-2$. The curvature θ_i (Equation 1), defined for each discrete step i along the trajectory (ranging from 1 to $T-2$, where T is the total number of sampled frames), is computed from the cosine similarity between successive displacement vectors Δz_i and Δz_{i+1}. This geometric relationship is visualized in Figure 3. The figure depicts three consecutive frame embeddings (z_i, z_{i+1}, z_{i+2}) from the overall dashed trajectory. The orange vectors Δz_i and Δz_{i+1} represent the displacements between these embeddings, with their respective lengths being the stepwise distances d_i and d_{i+1}. The green angle θ_i shows the turn at z_{i+1}. This angle, typically converted to degrees ($\theta_i^\circ = \theta_i \times \frac{180}{\pi}$), provides a measure of how sharply the representation trajectory bends at each step. These metrics, stepwise distance d_i and curvature θ_i, form the core of our geometric analysis.

4 Perceptual straightening of natural videos in DINOv2

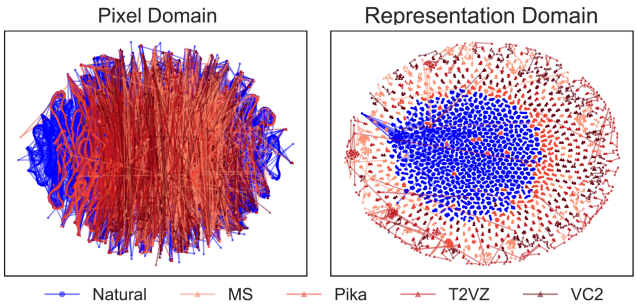

Figure 4: t-SNE embeddings of curvature trajectories for 1,000 videos from the VideoProM dataset [3]: 500 natural and 500 AI-generated (125 each from Pika [46], VideoCrafter2 [47], Text2Video-Zero [48], and ModelScope [49]; 24 frames/video). **Left (Pixel Space):** Natural and synthetic trajectories overlap significantly. **Right (DINOv2 ViT-S/14 Representation Space):** Trajectories clearly separate, with natural (blue) and AI-generated (shades of red) videos forming distinct clusters.

The classic finding is that visual system model have lower curvature in the representation space compared to pixel space–this is called *perceptual straightening* [1, 2]. For our application, we want to compare the relative curvature of natural and AI generated videos in any representational space. Just for simplicity, we could call this *real straightening* as in real videos are less curved than AI videos. One might expect that a model with good *perceptual straightening* also has good *real straightening*.

To test this hypothesis, we analyze fourteen vision encoders across diverse families: Supervised CNNs (AlexNet [50], VGG-16 [51], ResNet-50 [52], and the texture-debiased SIN-ResNet-50 [53]); Self-Supervised (SimCLR-R50 [54], BYOL-R50 [55], CLIP [56], and DINOv2 [25]); Human Visual System-Inspired (a Gabor Filter Bank [57] and the LGN-V1 model [1]); Spatio-temporal (S3d [58], R(2+1)D [59], and MViT [60]); and an Adversarially Trained ResNet-50 [61]. Surprisingly, as shown in Fig. 2B, we observe that the opposite seems to be the case: good perceptual straighteners actually make natural videos more curved than AI videos. HVS-inspired models achieve the strongest absolute straightening but do so indiscriminately for both real and AI videos, resulting in a negative curvature gap ($\Delta\theta < 0$). In contrast, self-supervised models like DINOv2 reduce the curvature of natural videos, which align with their learned priors of real-world statistics, but do not regularize the trajectories of AI-generated videos, which violate these priors. This differential response creates a large, positive curvature gap ($\Delta\theta = 45.46^\circ$ for DINOv2), which is the foundation of our method's success. The negligible correlation between absolute straightening and detection capability ($\rho = -0.13, p = 0.64$) confirms that detection performance hinges not on absolute straightening capability,

but on *differentially* straightening natural versus synthetic videos. While artificial neural networks may not fully replicate the absolute perceptual straightening observed in the biological visual system [24], this *relative* effect is the key mechanism for our detection method.

This principle is clearly visualized in Fig. 2A. Using matched pairs of real videos from Physics-IQ [26] and their AI-generated replicas, we see that geometric metrics overlap considerably in raw pixel space. However, in DINOv2's representation space, the trajectories separate distinctly, offering a clean signal for detection. Further evidence is provided in Fig. 4, which shows that this separation holds on a larger diverse dataset (VideoProM [3]). The t-SNE embeddings of curvature trajectories show natural videos (blue) forming a tight cluster, well-separated from the clusters of AI-generated videos (shades of red). This demonstrates that DINOv2's features effectively surface temporal inconsistencies without any task-specific training. Refer to Section A.1 for trajectories samples.

To implement this, we extract $T = 24$ frames $\mathcal{Z} = (z_1, \ldots, z_{24})$ by sampling over a 2-second video duration. This 2-second window is suitable for the videos considered in Section 7 ($\approx 2-5$s long with $12-30$ FPS), with an temporal based sample frame of $\Delta t = 2\text{s}/(24-1)$. Nevertheless, we hypothesize that using longer videos could further enhance performance. Our choice of a $2s$ window with 24 frames was found to provide an optimal trade-off between high detection accuracy and computational efficiency, as validated in our ablation studies (see B for details). Each x_i is resized to 224×224 pixels and normalized to $[0, 1]$. These preprocessed frames are then encoded by the DINOv2 ViT-S/14 model [25]. The 384 CLS (Classify) tokens and 196 patch embedding ($16 * 16$ patches of the $224 * 224$ inputs) from its final transformer block (`block.11`). These token embeddings are then flattened and concatenated to form a single feature vector $z_i \in \mathbb{R}^{75648}$. The sequence of these vectors, $\mathcal{Z}$, forms the temporal trajectory in DINOv2's representation space, from which temporal curvature and distance metrics are computed (Eq. (1)).

Takeaway 1: By projecting videos into DINOv2's representation space, geometric trajectory features (curvature & distance, Eq. 1) become indicators of synthetic origin, differentiating AI-generated videos from natural ones in a way that is not possible in raw pixel space.

5 Analyzing characteristics of perceptual trajectories

In order to analyze the differences of natural video trajectory signals vs. AI-generated ones we defined statistical features as the first four descriptive moments of both distance and curvature: mean, minimum, maximum and variance. This yields an 8-dimensional feature vector: $\left[\mu_d, \min d, \max d, \sigma_d^2, \mu_\theta, \min \theta, \max \theta, \sigma_\theta^2\right]$, where $\mu_d = \frac{1}{T-1}\sum_i d_i$ and $\sigma_d^2 = \frac{1}{T-1}\sum_i (d_i - \mu_d)^2$ (analogously for curvature θ_i°).

We select 50,000 AI-generated samples (10,000 each from Pika [46], VideoCraft2 [62], Text2Video-Zero [63], ModelScope [3], and Sora [64]) from VideoProM [3]. Concurrently, 50,000 natural videos are randomly chosen from DVSC2023 [47]. All videos are DINOv2 (ViT-S/14) encoded, and their aggregated statistical features are computed. Fig. 5 illustrates these aggregated feature distributions. The top row shows distance features ($\mu_d, \min_d, \max_d, \sigma_d^2$), characterizing inter-frame change magnitude and variability. The bottom row presents corresponding curvature features ($\mu_\theta, \min_\theta, \max_\theta, \sigma_\theta^2$), reflecting angular changes between consecutive frame transitions.

Statistical tests further confirm these observed differences. A two-sample t-test comparing the mean per-video μ between natural and AI-generated videos produced highly significant results. Distance (d): $t = -14.27,\ p = 5.53 \times 10^{-46}$; Curvature ($\theta$): $t = -44.02,\ p \approx 0$. An ANOVA comparing feature distributions among different AI generators and natural videos also shows strong statistical differentiation in DINOv2 embedding space (F-value of 18598.17, $p \approx 0$). These observations support our hypothesis: natural videos exhibit smoother, more consistent trajectories (lower μ_θ, surprisingly higher σ_θ^2), while AI-generated videos show irregular transitions resulting in higher curvature metrics but with lower σ_θ^2. These differences form the basis for our classification pipeline, where a classifier learns to separate natural from AI videos based on their trajectory geometry.

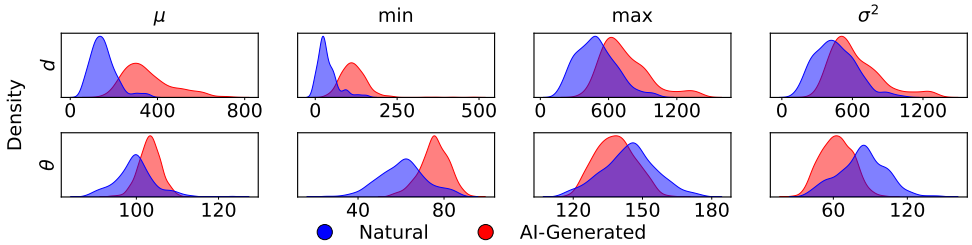

Figure 5: Distributions of aggregated temporal trajectory features (mean, min, max, variance) for natural and AI-generated videos, computed using DINOv2 ViT-S/14 representations. **Top row:** Temporal distance-based features (d_i). **Bottom row:** Corresponding curvature-based features (θ_i°). Both distance- and curvature-based features provide discriminative signal.

6 Video classifier to detect AI-generated content

Given that DINOv2 representation distance d and curvature θ differs significantly between natural and AI-generated videos, we evaluate if these features can be used in a lightweight, transparent, and easily replicated classifier without raw pixel processing or DINOv2 fine-tuning. We use the dataset from Section 5 and apply a stratified 50/50 train/test split. Class priors are identical, and each subset is balanced among five AI models (Pika [46], VideoCraft2 [62], Text2Video-Zero [63], ModelScope [3] and Sora [64]). We sample frames and we obtain the signals of distance $\{d_i\}_{i=1}^{T-1}$ and curvature $\{\theta_i^\circ\}_{i=1}^{T-2}$ as detailed in Section 5. For classification, we construct a feature vector y per video by combining direct signals and aggregated statistics from these trajectories. Specifically, y concatenates seven distance values $[d_1, d_2, \ldots, d_7]$ and six curvature values: $[\theta_1^\circ, \theta_2^\circ, \ldots, \theta_6^\circ]$; and four statistical descriptors (mean, variance, minimum, maximum) for both $\{d_i\}$ and $\{\theta_i^\circ\}$. This results in a final feature vector $y \in \mathbb{R}^{21}$. To ensure our curvature-based features are detecting generative artifacts rather than hard scene cut frequency, we performed a robustness analysis detailed in Section C.

We consider only off-the-shelf models: logistic regression (LR), Gaussian Naive Bayes (GNB), random forest (RF; 400 trees, depth ≤ 6), gradient boosting (GB; 200 rounds, learning rate 0.1), RBF-kernel SVM (calibrated by Platt scaling), and a two-layer MLP $(64 \rightarrow 32)$. We perform no feature engineering or hyperparameter search beyond a 3-fold grid/random sweep. For each classifier, we optimize the decision threshold τ^* on the training set to maximize the F_1-score. The chosen threshold τ^* was then applied unchanged to the test set. Inference cost is reported end-to-end (latency $= T_{\text{DINOv2}} + T_{\text{clf}}$), averaged over the test fold on a single NVIDIA RTX-2080 (see Section D). A DINOv2 forward pass (ViT-S/14, block 11, 8-frame batch) takes 43.6 ms. This constant is added to each classifier time (T_{clf}) in Table 1.

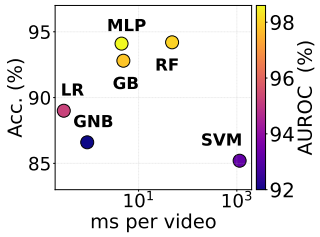

Figure 6: Inference-time (ms) vs. accuracy (%) and AUROC (%) for *ReStraV*'s classifiers.

Table 1: Performance and inference time of *ReStraV*'s classifiers, balanced 50k/50k natural/AI-generated video test set from VideoProM [3], cf. Section 5 for details. The best scores are **bold**, second best are underlined and the best method overall is highlighted in **blue**.

Model	Acc.	Bal.	Spec.	Pr_{gen}	Re_{gen}	F1_{gen}	AUROC	Time (ms)
SVM	85.23	85.78	86.42	96.93	85.04	90.62	93.27	1183.94
GNB	86.64	84.43	81.12	95.94	87.72	91.68	92.05	44.53
LR	89.02	88.86	88.53	97.54	89.17	93.12	95.26	**43.97**
GB	92.83	92.31	91.57	98.25	93.16	95.63	97.85	48.59
RF	**94.24**	88.67	80.37	96.13	**97.05**	**96.53**	98.03	48.14
MLP	94.17	**94.19**	**94.11**	**98.88**	94.14	96.48	**98.63**	48.12

Table 1 summarizes test performance. The MLP achieves the highest accuracy (94.17%), F_1-score (96.48%), and AUROC (98.6%) (Fig. 9A), followed by RF. Section 6 visualizes each classifier's speed/accuracy. Models in the upper-left offer the best cost/benefit. The MLP (highlighted blue in Table 1) achieves top AUROC and F_1 while being within ≈2ms from GNB. The confusion matrices and ROC (Fig. 9A and B in Section A.2) confirms low false positive/negative rates (cf. Section A.2

for decision boundaries visualization). Refer to Section A.3 for permutation feature importance analysis.

Takeaway 2: Simple, lightweight classifiers trained directly on geometric trajectory features achieve high classification accuracy ($\approx 94\%$) and AUROC ($\approx 99\%$), offering an efficient detection approach (≈ 48 ms per video) without complex modeling.

7 Benchmark results

We evaluate *ReStraV* (with MLP from Section 6) under four settings: **A)** Vs. SoTA image-based detectors on VidProM [3]; **B)** Vs. SoTA video detectors on VidProM [3] (evaluating "seen", "unseen", and "future" generator scenarios) and on the GenVidBench [17] dataset (in "cross-source"/"generator" (M) scenarios and its "Plants" hard task subclass (P)); **C)** Extreme generalization tests including one-to-many detection on the DeMamba [43] benchmark [43] and **D)** zero-shot evaluation on the Veo3 model [65]; **E)** Vs. a Vision-Language Model (VLM) performance (Gemini 1.5 Pro [66]) on the Physics-IQ dataset [26] using matched real/generated video pairs. The best scores are **bold**, second best are underlined and the best method overall is highlighted in **blue**.

A) ReStraV vs. image-based detectors. We evaluate our method *ReStraV* against eight SoTA image based detectors in Table 2. *ReStraV* is trained with data and processing from Section 6. We use a balanced test set (40,000 real videos; 10,000 AI-generated for each of four models: Pika [46], VideoCraft2 [67], Text2Video-Zero [48], ModelScope [49], replicating [3]'s implementation.

Performance is measured by overall classification accuracy and mean Average Precision (mAP). Table 2 summarizes the results from [3]. Baseline methods achieve moderate accuracies (45%–62%), with LNP [31] and Fusing [28] showing lower values. In contrast, our method obtains 97.06% average accuracy (Pika: 90.90%, VideoCraft2: 99.50%, Text2Video-Zero: 99.05%, ModelScope: 98.37%). *Caveat:* Comparing *ReStraV* to image-based detectors on a video task is not an even comparison (see next section for stronger baselines), yet it highlights the inadequacy of methods that rely solely on image-based features for AI-generated video detection neglecting temporal information.

Table 2: Comparison of *ReStraV* vs. image-based detectors on VidProM [3]. Accuracy (%) (left) and mAP (%) (right). Higher values (darker blue) indicate better performance. ↑ Higher is better.

	Accuracy ↑ (%)					**mAP** ↑ (%)				
Method	Pika	VC2	T2VZ	MS	Avg	Pika	VC2	T2VZ	MS	Avg
CNNSpot [27]	51.17	50.18	49.97	50.31	50.41	54.63	41.12	44.56	46.95	46.82
FreDect [29]	50.07	54.03	69.88	69.94	60.98	47.82	56.67	75.31	64.15	60.99
Fusing [28]	50.60	50.07	49.81	51.28	50.44	57.64	41.64	40.51	56.09	48.97
Gram-Net [16]	84.19	67.42	52.48	50.46	63.64	94.32	80.72	57.73	43.54	69.08
GIA [30]	53.73	51.75	41.05	60.22	51.69	54.49	53.21	36.69	66.53	52.73
LNP [31]	43.48	45.10	47.50	45.21	45.32	44.28	44.08	46.81	39.62	43.70
DFD [32]	50.53	49.95	48.96	48.32	49.44	49.21	50.44	44.52	48.64	48.20
UnivFD [33]	49.41	48.65	49.58	57.43	51.27	48.63	42.36	48.46	70.75	52.55
ReStraV	**90.90**	**99.50**	**99.05**	**98.37**	**97.06**	**99.12**	**98.76**	**98.93**	**98.44**	**98.81**

B) ReStraV vs. video-based detectors. We firstly compare *ReStraV* against the widely recognized VideoSwinTiny [39] (implementation from [17]) on the VidProM [3], with data setup following Section 7. Our evaluation considers three scenarios: **Seen generators:** Models are trained and tested on videos from a pool of the same four AI generators in Section 7, using a balanced set of 80,000 videos with a 50/50 train/test split. **Unseen generators:** Generalization is assessed by training models while excluding two specific AI generators (e.g., VC2 [62] and T2VZ [48]), which are then used for testing. **Future generators:** To simulate encountering a novel advanced model, *ReStraV* (trained on older generators) is tested on Sora [68]. Accuracy and mAP results in Table 3.

We futher evaluate *ReStraV*'s vs. nine SoTA video based detectors in Table 4. We consider two settings: **Main (M)** task, which is designed to test generalization across generators. Detectors are

trained on videos from Pika [46], VideoCraft2 [67], Text2Video-Zero [48], ModelScope [49], and tested on MuseV [69], Stable Video Diffusion (SVD) [70], CogVideo [71], and Mora [72]. **Plants (P)** task, the most challenging subset from [17]. The challenge may arise from the complex and often stochastic nature (e.g., irregular leaf patterns, subtle wind movements), which can make generative artifacts less distinguishable from natural variations or harder for models to consistently detect (qualitative samples in Section A.4). We use the same setting of task (M) but focusing on videos of plants in the test set. Baseline's results from [17].

Across both the Main (M) and Plants (P) tasks, *ReStraV* consistently performs near or above the baseline. On the Main (M) task, it demonstrates strong accuracies against AI generators (MuseV 93.52%, SVD 94.01%, CogVideo 93.52%, Mora 92.97%) and robust performance on natural videos (HD-VG/130M 91.07%), achieving a 93.01% average accuracy.

This robustness extends to the challenging Plants (P) task, where *ReStraV* obtains accuracies of 95.06% (MuseV), 97.83% (SVD), 92.38% (CogVideo), 91.24% (Mora), and 93.31% (HD-VG/130M), leading to a 93.96% average. This success may be attributed to *ReStraV*'s ability to capture specific curvature patterns inherent to "Plants" videos, which differ from more general artifacts. *ReStraV* remains highly effective as visualized by its position relative to the baseline spread (Fig. 13 in Section A.5).

Table 3: *ReStraV* vs. VideoSwin [39] fake video detection on VidProM[3]. "Seen generators" are those included in training; "Unseen generators" and "Future generators" were excluded from training. ↑ is better.

Condition	VideoSwin [39]	ReStraV (MLP)
Seen generators	Acc: 77.91 mAP: 75.33	**97.05** **98.78**
Unseen generators ([62, 63])	Acc: 62.44 mAP: 59.61	**89.45** **97.32**
Future generators (Sora [68])	Acc: 60.70 mAP: 58.20	**80.05** **92.85**

Table 4: Acc. (%) results of *ReStraV* vs. SoTA video based methods on the GenVidBench [17]. Table (a) shows results for the Main (M) task, and Table (b) for the Plants (P) task. ↑ is better.

(a) GenVidBench - Main (M) Task Acc. (%)

Method	MuseV	SVD	CogVideo	Mora	HD-VG [Nat.]	Avg.
TSM [34]	70.37	54.70	78.46	70.37	96.76	76.40
X3D [37]	92.39	37.27	65.72	49.60	97.51	77.09
MVIT V2 [38]	76.34	**98.29**	47.50	**96.62**	97.58	79.90
SlowFast [36]	12.25	12.68	38.34	45.93	93.63	41.66
I3D [35]	8.15	8.29	60.11	59.24	93.99	49.23
VideoSwin [39]	62.29	8.01	91.82	45.83	**99.29**	67.27
ReStraV	**93.52**	94.01	**93.52**	**92.97**	91.07	**93.01**

(b) GenVidBench - Plants (P) Task Acc. (%)

Method	MuseV	SVD	CogVideo	Mora	HD-VG [Nat.]	Avg.
SlowFast [36]	81.63	29.80	75.31	19.31	73.03	55.30
I3D [35]	39.18	23.27	91.98	78.38	78.42	62.15
VideoSwin [39]	57.96	7.35	92.59	47.88	**98.76**	52.86
TPN [40]	43.67	20.00	85.80	86.87	94.61	64.24
UniFormer V2 [41]	13.88	7.76	41.98	**95.75**	97.93	64.76
TimeSformer [42]	77.96	29.80	**96.30**	93.44	87.14	75.09
ReStraV	**95.06**	**97.83**	92.38	91.24	93.31	**96.96**

C) One-to-many generalization Test. We reproduced the one-to-many task from DeMamba [43], training on a single generator and testing on multiple unseen ones (Sora [68], MorphStudio [73], Gen2 [74], HotShot [75], Lavie [5], Show [76], MoonValley [77], Crafter [67], ModelScope [49] and WildScrape[43]). Table 5 shows average results across three training conditions. Notably, *ReStraV* achieves competitive or superior scores in most scenarios against specialized video detectors (TALL [78], NPR [79], STIL [80], and DeMamba [43]) using only the extracted trajectories.

D) Zero-shot Generalization Test. We tested zero-shot generalization on Google's Veo3 [65], a state-of-the-art model acclaimed for its ability to generate videos with plausible physical interations and consistent object interactions (qualitative frame samples in Section A.6). Using only the MLP trained in Section 6 (without any Veo3 videos in training), we

Table 5: One-to-many: training on one generator, testing on unseen generators (Sora, MorphStudio, Gen2, HotShot, Lavie, Show-1, MoonValley, Crafter, ModelScope, WildScrape). Avarage results from DeMamba benchmark [43]. ↑ is better.

	Train: Pika			Train: SEINE			Train: OpenSora		
Method	R	F1	AP	R	F1	AP	R	F1	AP
NPR	0.514	0.531	0.650	0.462	0.539	0.611	0.593	0.523	0.576
STIL	0.738	0.517	0.630	0.724	0.506	0.608	0.434	0.489	0.526
TALL	0.714	0.557	0.623	0.657	0.609	0.681	0.492	0.532	0.571
DeMamba	**0.757**	0.726	**0.817**	0.810	0.787	**0.894**	0.738	0.671	**0.738**
ReStraV	0.735	**0.827**	0.797	**0.820**	**0.898**	0.854	**0.771**	**0.797**	0.717

tested on 200 Veo3 versus 200 natural video pairs and achieved 83.2% accuracy, 85.1% F1, and 86.9% AUROC. This shows that the curvature-based detection signal can generalizes to future generators not represented in the training distribution, supporting our hypothesis that current generative models fundamentally struggle to replicate the temporal smoothness characteristic of natural world dynamics in learned representation spaces.

E) ReStraV vs. VLM detector on Physics-IQ dataset (matched real and generated videos). As a third and perhaps the most challenging test, we assess *ReStraV* on *matched* pairs of natural and generated videos from the Physics-IQ dataset. This dataset consists of real-world physical interactions and is special in the sense that it consists of both natural and AI-generated videos (198 per source) that are based on the very same starting frame(s): identical scenes, identical objects, identical lighting conditions as described in Section 5. We report [26]'s evaluation using a two-alternative forced-choice (2AFC) paradigm (a gold-standard psychophysical protocol). In each trial, a model sees a pair of videos: one real, one AI-generated.

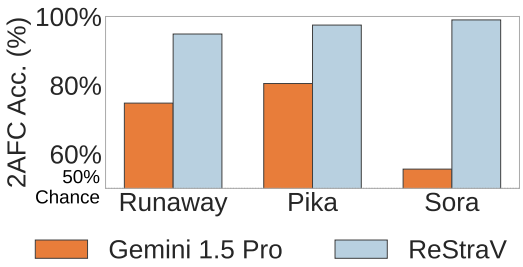

Figure 7: Fake video detection on Physics-IQ (*matched* real/generated video pairs). Gemini results from [26]. Despite the challenging task, ReStraV reliably identifies fake videos.

The task of identifying the AI-generated video is especially challenging due to the matched video nature. Motamed et al. [26] report results for a VLM, Gemini 1.5 Pro [66]. Gemini identifies Runway and Pika videos with reasonable accuracy (74.8% and 80.5% respectively), but Sora videos prove challenging (55.6%, near 50% chance) due to their photorealism.

We evaluate *ReStraV* in the same setting, comparing against reported numbers [26]. We compute mean aggregated video curvature (Eq. (1)) for each video and predict the one with higher mean curvature as "AI-generated." No further classifier training or calibration is performed. Fig. 7 shows the results: *ReStraV* attains 97.5% for Pika [46], 94.9% for Runway [81], and 99.0% for Sora. This near-perfect performance across all three generators demonstrates that simple curvature statistics robustly discriminate real from generated videos without model fine-tuning.

Takeaway 3: *ReStraV* demonstrates robust generalization across diverse generators and OOD scenarios, showing neural representation trajectories (distance d and curvature θ) as an effective paradigm for AI video detection.

8 Discussion

Summary. As AI-generated videos look more and more realistic, it is increasingly important to develop methods that reliably detect AI-generated content. We here propose using simple statistics such as the angle between video frame representations, inspired by the perceptual straightening hypothesis from neuroscience [1], to distinguish natural from generated videos. The approach is compellingly simple, fast, cheap, and surprisingly effective: using a pre-trained feature space such as DinoV2, the resulting "fake video" signal reliably identifies generated videos with high accuracies, setting a new SoTA in fake video identification.

The surprising observation that natural videos have, on average, less curvature but at the same time a *higher* variance in their curvature demands attention. Prior work found that temporal transitions in natural videos latent representations follow highly sparse distributions [82]. That means most of the time there is very little change, but sometimes a large jump. In terms of curvature, this could mean that most of the time, natural videos follow a relatively straight line through representation space, but sometimes take a sharp term (perhaps a scene cut). Further investigation in trajectory geometry (e.g., curvature kurtosis) will help to shed light on this in future work.

Implications for neuroscience. The finding that natural videos trace *straighter* paths than AI-generated ones in a frozen vision transformer dovetails with the *perceptual straightening* phenomenon reported in perceptual decision tasks and brain recordings [1, 2]. In the brain, such straightening is often interpreted as a by-product of predictive coding: when the visual system internalizes the physical regularities of its environment, successive latent states become easier to extrapolate, reducing curvature in representation space. Our results imply that even task-agnostic, self-supervised networks acquire a comparable inductive bias—suggesting a shared computational pressure, across biological and artificial systems, to encode "intuitive physics" in a geometry that favors smooth trajectories [83].

Naturalistic straightening offers a concrete, quantitative handle for probing world-model formation in neural populations. Future work could ask whether curvature statistics in cortical population codes track the degree of physical realism in controlled stimuli, or whether manipulations that disrupt intuitive physics (e.g., gravity-defying motion) elicit the same curvature inflation we observe in synthetic videos. Such experiments would clarify whether the brain genuinely leverages trajectory geometry as an error-monitoring signal and how this relates to theories of disentangled, factorized latent representations of dynamics.

Our method is invariant to playing a video backwards. This is clearly unnatural, if things, e.g., fall up instead of down; though at the same time this also would not be an instance of an AI-generated video. The arrow of time [84–86] can be a strong signal, but our metric is invariant to a reversal of time.

Limitations. Goodhart's law states that *"when a measure becomes a target, it ceases to be a good measure"*. Likewise, in the context of fake video detection, it is conceivable that someone developing a video model could train it in a way that optimizes for deceiving detection measures. This concern generally applies to all public detection methods, including ours. As a possible mitigation strategy, it may be helpful to employ several detection methods in tandem, since it may be harder to game multiple metrics simultaneously without sacrificing video quality. Furthermore, as video models become more and more capable of generating realistic, natural-looking videos, it is possible that future video models may not show the same statistical discrepancies between real and generated videos anymore, though this is hard to predict in advance.

Broader Impacts AI-generated video increasingly fuels fake news and disinformation [15]. *ReStraV* aims to positively impact this by enhancing content authentication. With AI-driven fraud like deepfake scams reportedly surging (e.g., a reported 2137% rise in financial sector attempts over three years [87]), efficient detection methods like *ReStraV* are becoming fundamental.

However, deploying detection technologies like *ReStraV* faces an "arms race" with evolving generation methods (see Limitations; also [22]). Additionally, biases inherited from pre-trained encoders (e.g., DINOv2 [25]) may cause fairness issues across diverse content [88]. Mitigating these risks demands ongoing research, transparency about limitations, and using detectors primarily to aid human judgment. Key strategies include careful contextual deployment, rigorous bias auditing and debiasing efforts [88], promoting media literacy [15], and advancing complementary methods like robust content watermarking [20].

The importance of AI-safety measures [89] is increasingly reflected in policy initiatives like the Coalition for Content Provenance and Authenticity [90] and the EU AI Act [91], both vital for a trustworthy digital ecosystem. However, deploying detection tools at scale presents its own challenges, especially concerning user privacy. To address this, detectors can be distributed and trained using privacy-by-design principles [92–94]. Within this framework, tools like *ReStraV* are crucial for ensuring the digital ecosystem remains grounded in reality, providing a critical defense against the long-term risk of epistemic decay in world models [95, 96].

Acknowledgements

This research was partly funded by Honda Research Institute Europe and Cold Spring Harbor Laboratory. We would like to thank Eero Simoncelli for insightful discussions and feedback, as well as Habon Issa, Filip Vercruysse, CiCi Xingyu Zheng, Alexei Koulakov, Andrea Castellani, Sebastian Schmitt, Andrea Moleri, Xavier Bonet-Monroig, Linus Ekstrøm, Riza Velioglu, Riccardo Cadei, and Christopher Van Buren for their helpful suggestions during the preparation of this manuscript, and Elena Ziegler for the appendix art illustration.

References

[1] Olivier J Hénaff, Robbe LT Goris, and Eero P Simoncelli. Perceptual straightening of natural videos. *Nature neuroscience*, 22(6):984–991, 2019.

[2] Olivier J Hénaff, Yoon Bai, Julie A Charlton, Ian Nauhaus, Eero P Simoncelli, and Robbe LT Goris. Primary visual cortex straightens natural video trajectories. *Nature communications*, 12 (1):5982, 2021.

[3] Wenhao Wang and Yi Yang. Vidprom: A million-scale real prompt-gallery dataset for text-to-video diffusion models, 2024. URL https://openreview.net/forum?id=pYNl76onJL.

[4] Yingqing He, Tianyu Yang, Yong Zhang, Ying Shan, and Qifeng Chen. Latent video diffusion models for high-fidelity long video generation, 2023. URL https://arxiv.org/abs/2211.13221.

[5] Yaohui Wang, Xinyuan Chen, Xin Ma, Shangchen Zhou, Ziqi Huang, Yi Wang, Ceyuan Yang, Yinan He, Jiashuo Yu, Peiqing Yang, Yuwei Guo, Tianxing Wu, Chenyang Si, Yuming Jiang, Cunjian Chen, Chen Change Loy, Bo Dai, Dahua Lin, Yu Qiao, and Ziwei Liu. Lavie: High-quality video generation with cascaded latent diffusion models, 2023. URL https://arxiv.org/abs/2309.15103.

[6] Pengyuan Zhou, Lin Wang, Zhi Liu, Yanbin Hao, Pan Hui, Sasu Tarkoma, and Jussi Kangasharju. A survey on generative ai and llm for video generation, understanding, and streaming. *ArXiv*, abs/2404.16038, 2024. URL https://api.semanticscholar.org/CorpusID:269362618.

[7] Sergey Tulyakov, Ming-Yu Liu, Xiaodong Yang, and Jan Kautz. Mocogan: Decomposing motion and content for video generation. In *2018 IEEE/CVF Conference on Computer Vision and Pattern Recognition*, pages 1526–1535, 2018. doi: 10.1109/CVPR.2018.00165.

[8] Mengyu Chu, You Xie, Jonas Mayer, Laura Leal-Taixé, and Nils Thuerey. Learning temporal coherence via self-supervision for gan-based video generation. *ACM Trans. Graph.*, 39(4), August 2020. ISSN 0730-0301. doi: 10.1145/3386569.3392457. URL https://doi.org/10.1145/3386569.3392457.

[9] Anne Harrington, Vasha DuTell, Ayush Tewari, Mark Hamilton, Simon Stent, Ruth Rosenholtz, and William T. Freeman. Exploring perceptual straightness in learned visual representations. In *The Eleventh International Conference on Learning Representations*, 2023. URL https://openreview.net/forum?id=4cOfD2qL6T.

[10] Neelu Madan, Andreas Moegelmose, Rajat Modi, Yogesh S. Rawat, and Thomas B. Moeslund. Foundation models for video understanding: A survey, 2024. URL https://arxiv.org/abs/2405.03770.

[11] Yimu Wang, Xuye Liu, Wei Pang, Li Ma, Shuai Yuan, Paul Debevec, and Ning Yu. Survey of video diffusion models: Foundations, implementations, and applications. *Transactions on Machine Learning Research*, 2025. ISSN 2835-8856. URL https://openreview.net/forum?id=2ODDBObKjH. Survey Certification.

[12] Jonathan Ho, Ajay Jain, and Pieter Abbeel. Denoising diffusion probabilistic models, 2020. URL https://arxiv.org/abs/2006.11239.

[13] Ashish Vaswani, Noam Shazeer, Niki Parmar, Jakob Uszkoreit, Llion Jones, Aidan N Gomez, Ł ukasz Kaiser, and Illia Polosukhin. Attention is all you need. In I. Guyon, U. Von Luxburg, S. Bengio, H. Wallach, R. Fergus, S. Vishwanathan, and R. Garnett, editors, *Advances in Neural Information Processing Systems*, volume 30. Curran Associates, Inc., 2017. URL https://proceedings.neurips.cc/paper_files/paper/2017/file/3f5ee243547dee91fbd053c1c4a845aa-Paper.pdf.

[14] Alexey Dosovitskiy, Lucas Beyer, Alexander Kolesnikov, Dirk Weissenborn, Xiaohua Zhai, Thomas Unterthiner, Mostafa Dehghani, Matthias Minderer, Georg Heigold, Sylvain Gelly, Jakob Uszkoreit, and Neil Houlsby. An image is worth 16x16 words: Transformers for image recognition at scale, 2021. URL https://arxiv.org/abs/2010.11929.

[15] Bart van der Sloot and Yvette Wagensveld. Deepfakes: regulatory challenges for the synthetic society. *Computer Law & Security Review*, 46:105716, 2022. ISSN 2212-473X. doi: https://doi.org/10.1016/j.clsr.2022.105716. URL https://www.sciencedirect.com/science/article/pii/S0267364922000632.

[16] Zhengzhe Liu, Xiaojuan Qi, and Philip Torr. Global texture enhancement for fake face detection in the wild, 2020. URL https://arxiv.org/abs/2002.00133.

[17] Zhenliang Ni, Qiangyu Yan, Mouxiao Huang, Tianning Yuan, Yehui Tang, Hailin Hu, Xinghao Chen, and Yunhe Wang. Genvidbench: A challenging benchmark for detecting ai-generated video, 2025. URL https://arxiv.org/abs/2501.11340.

[18] Zhiyuan Yan, Yong Zhang, Xinhang Yuan, Siwei Lyu, and Baoyuan Wu. Deepfakebench: A comprehensive benchmark of deepfake detection, 2023. URL https://arxiv.org/abs/2307.01426.

[19] Md Asikuzzaman and Mark R Pickering. An overview of digital video watermarking. *IEEE Transactions on Circuits and Systems for Video Technology*, 28(9):2131–2153, 2017.

[20] Sumanth Dathathri, Abigail See, Sumedh Ghaisas, Po-Sen Huang, Rob McAdam, Johannes Welbl, Vandana Bachani, Alex Kaskasoli, Robert Stanforth, Tatiana Matejovicova, et al. Scalable watermarking for identifying large language model outputs. *Nature*, 634(8035): 818–823, 2024.

[21] S. Craver, N. Memon, B.-L. Yeo, and M.M. Yeung. Resolving rightful ownerships with invisible watermarking techniques: limitations, attacks, and implications. *IEEE Journal on Selected Areas in Communications*, 16(4):573–586, 1998. doi: 10.1109/49.668979.

[22] Hanlin Zhang, Benjamin L. Edelman, Danilo Francati, Daniele Venturi, Giuseppe Ateniese, and Boaz Barak. Watermarks in the sand: Impossibility of strong watermarking for generative models, 2025. URL https://arxiv.org/abs/2311.04378.

[23] Eghbal Hosseini and Evelina Fedorenko. Large language models implicitly learn to straighten neural sentence trajectories to construct a predictive representation of natural language. In A. Oh, T. Naumann, A. Globerson, K. Saenko, M. Hardt, and S. Levine, editors, *Advances in Neural Information Processing Systems*, volume 36, pages 43918–43930. Curran Associates, Inc., 2023. URL https://proceedings.neurips.cc/paper_files/paper/2023/file/88dddaf430b5bc38ab8228902bb61821-Paper-Conference.pdf.

[24] Xueyan Niu, Cristina Savin, and Eero P Simoncelli. Learning predictable and robust neural representations by straightening image sequences. In *The Thirty-eighth Annual Conference on Neural Information Processing Systems*, 2024. URL https://openreview.net/forum?id=fYfliutfHX.

[25] Maxime Oquab, Timothée Darcet, Théo Moutakanni, Huy V. Vo, Marc Szafraniec, Vasil Khalidov, Pierre Fernandez, Daniel HAZIZA, Francisco Massa, Alaaeldin El-Nouby, Mido Assran, Nicolas Ballas, Wojciech Galuba, Russell Howes, Po-Yao Huang, Shang-Wen Li, Ishan Misra, Michael Rabbat, Vasu Sharma, Gabriel Synnaeve, Hu Xu, Herve Jegou, Julien Mairal, Patrick Labatut, Armand Joulin, and Piotr Bojanowski. DINOv2: Learning robust visual features without supervision. *Transactions on Machine Learning Research*, 2024. ISSN 2835-8856. URL https://openreview.net/forum?id=a68SUt6zFt. Featured Certification.

[26] Saman Motamed, Laura Culp, Kevin Swersky, Priyank Jaini, and Robert Geirhos. Do generative video models understand physical principles?, 2025. URL https://arxiv.org/abs/2501.09038.

[27] You-Ming Chang, Chen Yeh, Wei-Chen Chiu, and Ning Yu. Antifakeprompt: Prompt-tuned vision-language models are fake image detectors, 2024. URL https://arxiv.org/abs/2310.17419.

[28] Sheng-Yu Wang, Oliver Wang, Richard Zhang, Andrew Owens, and Alexei A. Efros. Cnn-generated images are surprisingly easy to spot... for now, 2020. URL https://arxiv.org/abs/1912.11035.

[29] Chandler Timm Doloriel and Ngai-Man Cheung. Frequency masking for universal deepfake detection, 2024. URL https://arxiv.org/abs/2401.06506.

[30] Joel Frank, Thorsten Eisenhofer, Lea Schönherr, Asja Fischer, Dorothea Kolossa, and Thorsten Holz. Leveraging frequency analysis for deep fake image recognition, 2020. URL https://arxiv.org/abs/2003.08685.

[31] Chuangchuang Tan, Yao Zhao, Shikui Wei, Guanghua Gu, and Yunchao Wei. Learning on gradients: Generalized artifacts representation for gan-generated images detection. In *2023 IEEE/CVF Conference on Computer Vision and Pattern Recognition (CVPR)*, pages 12105–12114, 2023. doi: 10.1109/CVPR52729.2023.01165.

[32] Xiuli Bi, Bo Liu, Fan Yang, Bin Xiao, Weisheng Li, Gao Huang, and Pamela C. Cosman. Detecting generated images by real images only, 2023. URL https://arxiv.org/abs/2311.00962.

[33] Utkarsh Ojha, Yuheng Li, and Yong Jae Lee. Towards universal fake image detectors that generalize across generative models, 2024. URL https://arxiv.org/abs/2302.10174.

[34] Ji Lin, Chuang Gan, and Song Han. Tsm: Temporal shift module for efficient video understanding, 2019. URL https://arxiv.org/abs/1811.08383.

[35] Joao Carreira and Andrew Zisserman. Quo vadis, action recognition? a new model and the kinetics dataset, 2018. URL https://arxiv.org/abs/1705.07750.

[36] Christoph Feichtenhofer, Haoqi Fan, Jitendra Malik, and Kaiming He. Slowfast networks for video recognition, 2019. URL https://arxiv.org/abs/1812.03982.

[37] Christoph Feichtenhofer. X3d: Expanding architectures for efficient video recognition. In *Proceedings of the IEEE/CVF conference on computer vision and pattern recognition*, pages 203–213, 2020.

[38] Yanghao Li, Chao-Yuan Wu, Haoqi Fan, Karttikeya Mangalam, Bo Xiong, Jitendra Malik, and Christoph Feichtenhofer. Mvitv2: Improved multiscale vision transformers for classification and detection. In *Proceedings of the IEEE/CVF conference on computer vision and pattern recognition*, pages 4804–4814, 2022.

[39] Ze Liu, Jia Ning, Yue Cao, Yixuan Wei, Zheng Zhang, Stephen Lin, and Han Hu. Video swin transformer. In *Proceedings of the IEEE/CVF Conference on Computer Vision and Pattern Recognition (CVPR)*, pages 3202–3211, June 2022.

[40] Ceyuan Yang, Yinghao Xu, Jianping Shi, Bo Dai, and Bolei Zhou. Temporal pyramid network for action recognition, 2020. URL https://arxiv.org/abs/2004.03548.

[41] Kunchang Li, Yali Wang, Yinan He, Yizhuo Li, Yi Wang, Limin Wang, and Yu Qiao. Uniformerv2: Spatiotemporal learning by arming image vits with video uniformer, 2022. URL https://arxiv.org/abs/2211.09552.

[42] Gedas Bertasius, Heng Wang, and Lorenzo Torresani. Is space-time attention all you need for video understanding?, 2021. URL https://arxiv.org/abs/2102.05095.

[43] Haoxing Chen, Yan Hong, Zizheng Huang, Zhuoer Xu, Zhangxuan Gu, Yaohui Li, Jun Lan, Huijia Zhu, Jianfu Zhang, Weiqiang Wang, and Huaxiong Li. Demamba: Ai-generated video detection on million-scale genvideo benchmark, 2024. URL https://arxiv.org/abs/2405.19707.

[44] Pavan C. Madhusudana, Neil Birkbeck, Yilin Wang, Balu Adsumilli, and Alan C. Bovik. St-greed: Space-time generalized entropic differences for frame rate dependent video quality prediction. *IEEE Transactions on Image Processing*, 30:7446–7457, 2021. ISSN 1941-0042. doi: 10.1109/tip.2021.3106801. URL http://dx.doi.org/10.1109/TIP.2021.3106801.

[45] Pavan C. Madhusudana, Neil Birkbeck, Yilin Wang, Balu Adsumilli, and Alan C. Bovik. Image quality assessment using contrastive learning. *IEEE Transactions on Image Processing*, 31:4149–4161, 2022. ISSN 1941-0042. doi: 10.1109/tip.2022.3181496. URL http://dx.doi.org/10.1109/TIP.2022.3181496.

[46] Pika Labs Team. Pika labs. Generative ai platform for creating video and visual content., 2024. URL https://pikalabs.com.

[47] Ed Pizzi, Giorgos Kordopatis-Zilos, Hiral Patel, Gheorghe Postelnicu, Sugosh Nagavara Ravindra, Akshay Gupta, Symeon Papadopoulos, Giorgos Tolias, and Matthijs Douze. The 2023 video similarity dataset and challenge. *Comput. Vis. Image Underst.*, 243:103997, 2024. URL https://doi.org/10.1016/j.cviu.2024.103997.

[48] Uriel Singer, Adam Polyak, Thomas Hayes, Xi Yin, Jie An, Songyang Zhang, Qiyuan Hu, Harry Yang, Oron Ashual, Oran Gafni, Devi Parikh, Sonal Gupta, and Yaniv Taigman. Make-a-video: Text-to-video generation without text-video data, 2022. URL https://arxiv.org/abs/2209.14792.

[49] Jiuniu Wang, Hangjie Yuan, Dayou Chen, Yingya Zhang, Xiang Wang, and Shiwei Zhang. Modelscope text-to-video technical report, 2023. URL https://arxiv.org/abs/2308.06571.

[50] Alex Krizhevsky, Ilya Sutskever, and Geoffrey E Hinton. Imagenet classification with deep convolutional neural networks. In F. Pereira, C.J. Burges, L. Bottou, and K.Q. Weinberger, editors, *Advances in Neural Information Processing Systems*, volume 25. Curran Associates, Inc., 2012. URL https://proceedings.neurips.cc/paper_files/paper/2012/file/c399862d3b9d6b76c8436e924a68c45b-Paper.pdf.

[51] Karen Simonyan and Andrew Zisserman. Very deep convolutional networks for large-scale image recognition, 2015. URL https://arxiv.org/abs/1409.1556.

[52] Kaiming He, Xiangyu Zhang, Shaoqing Ren, and Jian Sun. Deep residual learning for image recognition. In *2016 IEEE Conference on Computer Vision and Pattern Recognition (CVPR)*, pages 770–778, 2016. doi: 10.1109/CVPR.2016.90.

[53] Robert Geirhos, Patricia Rubisch, Claudio Michaelis, Matthias Bethge, Felix Wichmann, and Wieland Brendel. Imagenet-trained cnns are biased towards texture; increasing shape bias improves accuracy and robustness. *ArXiv*, abs/1811.12231, 2018. URL https://api.semanticscholar.org/CorpusID:54101493.

[54] Ting Chen, Simon Kornblith, Mohammad Norouzi, and Geoffrey Hinton. A simple framework for contrastive learning of visual representations, 2020. URL https://arxiv.org/abs/2002.05709.

[55] Jean-Bastien Grill, Florian Strub, Florent Altché, Corentin Tallec, Pierre Richemond, Elena Buchatskaya, Carl Doersch, Bernardo Avila Pires, Zhaohan Guo, Mohammad Gheshlaghi Azar, Bilal Piot, koray kavukcuoglu, Remi Munos, and Michal Valko. Bootstrap your own latent - a new approach to self-supervised learning. In H. Larochelle, M. Ranzato, R. Hadsell, M.F. Balcan, and H. Lin, editors, *Advances in Neural Information Processing Systems*, volume 33, pages 21271–21284. Curran Associates, Inc., 2020. URL https://proceedings.neurips.cc/paper_files/paper/2020/file/f3ada80d5c4ee70142b17b8192b2958e-Paper.pdf.

[56] Alec Radford, Jong Wook Kim, Chris Hallacy, Aditya Ramesh, Gabriel Goh, Sandhini Agarwal, Girish Sastry, Amanda Askell, Pamela Mishkin, Jack Clark, Gretchen Krueger, and Ilya Sutskever. Learning transferable visual models from natural language supervision. In *International Conference on Machine Learning*, 2021. URL https://api.semanticscholar.org/CorpusID:231591445.

[57] J P Jones and Larry A Palmer. An evaluation of the two-dimensional gabor filter model of simple receptive fields in cat striate cortex. *Journal of neurophysiology*, 58 6:1233–58, 1987. URL https://api.semanticscholar.org/CorpusID:16809045.

[58] Saining Xie, Chen Sun, Jonathan Huang, Zhuowen Tu, and Kevin Murphy. Rethinking spatiotemporal feature learning: Speed-accuracy trade-offs in video classification, 2018. URL https://arxiv.org/abs/1712.04851.

[59] Kensho Hara, Hirokatsu Kataoka, and Yutaka Satoh. Can spatiotemporal 3d cnns retrace the history of 2d cnns and imagenet? In *2018 IEEE/CVF Conference on Computer Vision and Pattern Recognition*, pages 6546–6555, 2018. doi: 10.1109/CVPR.2018.00685.

[60] Haoqi Fan, Bo Xiong, Karttikeya Mangalam, Yanghao Li, Zhicheng Yan, Jitendra Malik, and Christoph Feichtenhofer. Multiscale vision transformers, 2021. URL https://arxiv.org/abs/2104.11227.

[61] Alex Harrington, Arturo Deza, Sarah Schwettmann, Konrad Kording, and Leila Wehbe. Exploring perceptual straightness in learned visual representations. In *ICLR*, 2023.

[62] Haoxin Chen, Yong Zhang, Xiaodong Cun, Menghan Xia, Xintao Wang, Chao Weng, and Ying Shan. Videocrafter2: Overcoming data limitations for high-quality video diffusion models, 2024. URL https://arxiv.org/abs/2401.09047.

[63] Levon Khachatryan, Andranik Movsisyan, Vahram Tadevosyan, Roberto Henschel, Zhangyang Wang, Shant Navasardyan, and Humphrey Shi. Text2video-zero: Text-to-image diffusion models are zero-shot video generators, 2023. URL https://arxiv.org/abs/2303.13439.

[64] OpenAI. Sora: OpenAI's Multimodal Agent. Sora: A review on background, technology, limitations, and opportunities of large vision models, 2024. URL https://openai.com/index/sora/.

[65] Google DeepMind. Veo 3. https://deepmind.google/technologies/veo/veo-3/, 2024.

[66] Gemini Team, Petko Georgiev, and 1133 other authors. Gemini 1.5: Unlocking multimodal understanding across millions of tokens of context, 2024. URL https://arxiv.org/abs/2403.05530.

[67] Haoxin Chen, Menghan Xia, Yingqing He, Yong Zhang, Xiaodong Cun, Shaoshu Yang, Jinbo Xing, Yaofang Liu, Qifeng Chen, Xintao Wang, Chao Weng, and Ying Shan. Videocrafter1: Open diffusion models for high-quality video generation, 2023. URL https://arxiv.org/abs/2310.19512.

[68] OpenAI. Sora: Video generation models as world simulators. https://openai.com, 2024.

[69] Huiwen Chang, Han Zhang, Jarred Barber, AJ Maschinot, Jose Lezama, Lu Jiang, Ming-Hsuan Yang, Kevin Murphy, William T. Freeman, Michael Rubinstein, Yuanzhen Li, and Dilip Krishnan. Muse: Text-to-image generation via masked generative transformers, 2023. URL https://arxiv.org/abs/2301.00704.

[70] Andreas Blattmann, Tim Dockhorn, Sumith Kulal, Daniel Mendelevitch, Maciej Kilian, Dominik Lorenz, Yam Levi, Zion English, Vikram Voleti, Adam Letts, Varun Jampani, and Robin Rombach. Stable video diffusion: Scaling latent video diffusion models to large datasets, 2023. URL https://arxiv.org/abs/2311.15127.

[71] Wenyi Hong, Ming Ding, Wendi Zheng, Xinghan Liu, and Jie Tang. Cogvideo: Large-scale pretraining for text-to-video generation via transformers, 2022. URL https://arxiv.org/abs/2205.15868.

[72] Zhengqing Yuan, Yixin Liu, Yihan Cao, Weixiang Sun, Haolong Jia, Ruoxi Chen, Zhaoxu Li, Bin Lin, Li Yuan, Lifang He, Chi Wang, Yanfang Ye, and Lichao Sun. Mora: Enabling generalist video generation via a multi-agent framework, 2024. URL https://arxiv.org/abs/2403.13248.

[73] Morph Studio. Morph studio text to video. https://www.morphstudio.com/, 2024. Accessed: 2025-10-03.

[74] Runway. Gen-2: The next step forward in generative ai. https://runwayml.com/blog/gen-2/, 2023. Accessed: 2025-10-03.

[75] Natural Selection Labs. Hotshot-xl model. https://huggingface.co/hotshotco/Hotshot-XL, 2023. Accessed: 2025-10-03.

[76] David Junhao Zhang, Jay Zhangjie Wu, Jia-Wei Liu, Rui Zhao, Lingmin Ran, Yuchao Gu, Difei Gao, and Mike Zheng Shou. Show-1: Marrying pixel and latent diffusion models for text-to-video generation, 2025. URL https://arxiv.org/abs/2309.15818.

[77] MoonValley. Moonvalley text to video generator. https://moonvalley.ai/, 2023. Accessed: 2025-10-03.

[78] Yuting Xu, Jian Liang, Gengyun Jia, Ziming Yang, Yanhao Zhang, and Ran He. Tall: Thumbnail layout for deepfake video detection, 2024. URL https://arxiv.org/abs/2307.07494.

[79] Chuangchuang Tan, Huan Liu, Yao Zhao, Shikui Wei, Guanghua Gu, Ping Liu, and Yunchao Wei. Rethinking the up-sampling operations in cnn-based generative network for generalizable deepfake detection. In *2024 IEEE/CVF Conference on Computer Vision and Pattern Recognition (CVPR)*, pages 28130–28139, 2024. doi: 10.1109/CVPR52733.2024.02657.

[80] Dengyong Zhang, Wenjie Zhu, Xin Liao, Feifan Qi, Gaobo Yang, and Xiangling Ding. Spatiotemporal inconsistency learning and interactive fusion for deepfake video detection. *ACM Trans. Multimedia Comput. Commun. Appl.*, 21(2), December 2024. ISSN 1551-6857. doi: 10.1145/3664654. URL https://doi.org/10.1145/3664654.

[81] Runway Team. Runway. Platform for ai-powered video editing and generative media creations, 2024. URL https://runwayml.com.

[82] David A. Klindt, Lukas Schott, Yash Sharma, Ivan Ustyuzhaninov, Wieland Brendel, Matthias Bethge, and Dylan Paiton. Towards nonlinear disentanglement in natural data with temporal sparse coding. In *International Conference on Learning Representations*, 2021. URL https://openreview.net/forum?id=EbIDjBynYJ8.

[83] Sarah Schwettmann, Jason Fischer, Joshua B. Tenenbaum, and Nancy G. Kanwisher. Evidence for an intuitive physics engine in the human brain. *Cognitive Science*, 2018. URL https://api.semanticscholar.org/CorpusID:86388528.

[84] David Danks. The psychology of causal perception and reasoning. In *The Oxford Handbook of Causation*. Oxford University Press, 11 2009. ISBN 9780199279739. doi: 10.1093/oxfordhb/9780199279739.003.0022. URL https://doi.org/10.1093/oxfordhb/9780199279739.003.0022.

[85] Donglai Wei, Joseph J Lim, Andrew Zisserman, and William T Freeman. Learning and using the arrow of time. In *Proceedings of the IEEE conference on computer vision and pattern recognition*, pages 8052–8060, 2018.

[86] Kristof Meding, Dominik Janzing, Bernhard Schölkopf, and Felix A. Wichmann. Perceiving the arrow of time in autoregressive motion. In H. Wallach, H. Larochelle, A. Beygelzimer, F. d'Alché-Buc, E. Fox, and R. Garnett, editors, *Advances in Neural Information Processing Systems*, volume 32. Curran Associates, Inc., 2019. URL https://proceedings.neurips.cc/paper_files/paper/2019/file/8d3369c4c086f236fabf61d614a32818-Paper.pdf.

[87] Ahmet Tulga. Fraud attempts with deepfakes have increased by 2137% over the last three years. Technical report, Signicat Press Releases, February 2025. Accessed May 2025.

[88] Uzoamaka Ezeakunne, Chrisantus Eze, and Xiuwen Liu. Data-driven fairness generalization for deepfake detection, 2024. URL https://arxiv.org/abs/2412.16428.

[89] Miles Brundage and Shahar et al. Avin. *The Malicious Use of Artificial Intelligence: Forecasting, Prevention, and Mitigation*. 2018. doi: 10.17863/CAM.22520. URL https://www.repository.cam.ac.uk/handle/1810/275332.

[90] Adobe and Arm and BBC and Intel and Microsoft and Truepic. The C2PA: An Open Standard for Content Provenance and Authenticity. Technical report, Coalition for Content Provenance and Authenticity (C2PA), sep 2020.

[91] Bram Rijsbosch, Gijs van Dijck, and Konrad Kollnig. Adoption of watermarking for generative ai systems in practice and implications under the new eu ai act, 2025. URL https://arxiv.org/abs/2503.18156.

[92] Brendan McMahan, Eider Moore, Daniel Ramage, Seth Hampson, and Blaise Aguera y Arcas. Communication-Efficient Learning of Deep Networks from Decentralized Data. In Aarti Singh and Jerry Zhu, editors, *Proceedings of the 20th International Conference on Artificial Intelligence and Statistics*, volume 54 of *Proceedings of Machine Learning Research*, pages 1273–1282. PMLR, 20–22 Apr 2017. URL https://proceedings.mlr.press/v54/mcmahan17a.html.

[93] Martin Abadi, Andy Chu, Ian Goodfellow, H. Brendan McMahan, Ilya Mironov, Kunal Talwar, and Li Zhang. Deep learning with differential privacy. In *Proceedings of the 2016 ACM SIGSAC Conference on Computer and Communications Security*, CCS '16, page 308–318, New York, NY, USA, 2016. Association for Computing Machinery. ISBN 9781450341394. doi: 10.1145/2976749.2978318. URL https://doi.org/10.1145/2976749.2978318.

[94] Christian Internò, Elena Raponi, Niki van Stein, Thomas Bäck, Markus Olhofer, Yaochu Jin, and Barbara Hammer. Adaptive hybrid model pruning in federated learning through loss exploration. In *International Workshop on Federated Foundation Models in Conjunction with NeurIPS 2024*, 2024. URL https://openreview.net/forum?id=OxpWu6J0TW.

[95] David Ha and Jürgen Schmidhuber. World models. 2018. doi: 10.5281/ZENODO.1207631. URL https://zenodo.org/record/1207631.

[96] Riccardo Cadei and Christian Internò. The narcissus hypothesis: Descending to the rung of illusion. In *NeurIPS 2025 Workshop on Evaluating the Evolving LLM Lifecycle: Benchmarks, Emergent Abilities, and Scaling*, 2025. URL https://openreview.net/forum?id=I9CJp7hcZI.

[97] Carl Vondrick, Hamed Pirsiavash, and Antonio Torralba. Generating videos with scene dynamics. In D. Lee, M. Sugiyama, U. Luxburg, I. Guyon, and R. Garnett, editors, *Advances in Neural Information Processing Systems*, volume 29. Curran Associates, Inc., 2016. URL https://proceedings.neurips.cc/paper_files/paper/2016/file/04025959b191f8f9de3f924f0940515f-Paper.pdf.

[98] Mohammad Babaeizadeh, Chelsea Finn, Dumitru Erhan, Roy H. Campbell, and Sergey Levine. Stochastic variational video prediction. In *International Conference on Learning Representations*, 2018. URL https://openreview.net/forum?id=rk49Mg-CW.

[99] Robin Rombach, Andreas Blattmann, Dominik Lorenz, Patrick Esser, and Bjorn Ommer. High-Resolution Image Synthesis with Latent Diffusion Models . In *2022 IEEE/CVF Conference on Computer Vision and Pattern Recognition (CVPR)*, pages 10674–10685, Los Alamitos, CA, USA, June 2022. IEEE Computer Society. doi: 10.1109/CVPR52688.2022.01042. URL https://doi.ieeecomputersociety.org/10.1109/CVPR52688.2022.01042.

[100] Jonathan Ho, William Chan, Chitwan Saharia, Jay Whang, Ruiqi Gao, Alexey Gritsenko, Diederik P. Kingma, Ben Poole, Mohammad Norouzi, David J. Fleet, and Tim Salimans. Imagen video: High definition video generation with diffusion models, 2022. URL https://arxiv.org/abs/2210.02303.

[101] Jiahao Shao, Yuanbo Yang, Hongyu Zhou, Youmin Zhang, Yujun Shen, Matteo Poggi, and Yiyi Liao. Learning temporally consistent video depth from video diffusion priors. *CoRR*, abs/2406.01493, 2024. URL https://doi.org/10.48550/arXiv.2406.01493.

[102] Dan Kondratyuk, Lijun Yu, Xiuye Gu, José Lezama, Jonathan Huang, Grant Schindler, Rachel Hornung, Vighnesh Birodkar, Jimmy Yan, Ming-Chang Chiu, Krishna Somandepalli, Hassan Akbari, Yair Alon, Yong Cheng, Josh Dillon, Agrim Gupta, Meera Hahn, Anja Hauth, David Hendon, Alonso Martinez, David Minnen, Mikhail Sirotenko, Kihyuk Sohn, Xuan

Yang, Hartwig Adam, Ming-Hsuan Yang, Irfan Essa, Huisheng Wang, David A. Ross, Bryan Seybold, and Lu Jiang. Videopoet: A large language model for zero-shot video generation, 2024. URL https://arxiv.org/abs/2312.14125.

[103] Bingyi Kang, Yang Yue, Rui Lu, Zhijie Lin, Yang Zhao, Kaixin Wang, Gao Huang, and Jiashi Feng. How far is video generation from world model: A physical law perspective, 2024. URL https://arxiv.org/abs/2411.02385.

[104] Xiaofeng Wang, Zheng Zhu, Guan Huang, Boyuan Wang, Xinze Chen, and Jiwen Lu. Worlddreamer: Towards general world models for video generation via predicting masked tokens, 2024. URL https://arxiv.org/abs/2401.09985.

[105] Brandon Castellano. PySceneDetect: A Python library and command-line tool for video scene detection. https://www.scenedetect.com, 2024. URL https://github.com/Breakthrough/PySceneDetect.

Appendix Contents

A AI Video Generation 20

A.1 Qualitative Examples of Perceptual Trajectories 20

A.2 ReStraV Classifiers Results Analysis 21

A.3 Feature Importance Analysis 22

A.4 Qualitative Examples of "Plants" Task 22

A.5 Results Distributions for Main Task (M) and Plants Task (P) 23

A.6 Frame Samples from the Veo3 Model for Zero-shot Generalization Test 23

B Ablation Studies 23

B.1 Impact of Video Length and Sampling Density 24

B.2 Robustness to Temporal Window Position 24

C Analysis of Scene Cut Frequency 26

D Computational Environment 26

E Dataset Licenses and Sources 26

A AI Video Generation

Early video generation used deep generative models like GANs and variational methods. [97] used VGANs for tiny video loops; [7] introduced MoCoGAN to separate motion and content. These pioneering methods, despite enabling synthetic video generation, often produced blurry or temporally incoherent results. [98] addressed future frame uncertainty with the Stochastic Variational Video Prediction (SV2P) model, using stochastic latent variables for diverse video sequences.

Diffusion models marked a significant breakthrough. Foundational methods like DDPM [12] (images) and Latent Diffusion [99] achieved high-fidelity generation via iterative denoising. Video Diffusion Models (VDMs) then addressed temporal consistency, e.g., using time-conditioned 3D U-Nets [100]. This led to prominent text-to-video systems like Imagen Video [100] and Make-A-Video [48], often using cascaded super-resolution. Latent diffusion variants like Text2Video-Zero [63] and ModelScope [3] improved efficiency by operating in latent spaces. Generative foundation models have diversified beyond diffusion. OpenAI's Sora [64] showed strong text-to-video capabilities using transformer decoders. Runway Gen-3 [81] uses autoregressive generation for temporal dynamics; Pika [46] combines diffusion and autoregressive decoding for improved coherence and quality.

Despite these advances, robust temporal consistency and physical plausibility remain significant challenges. Temporal inconsistencies occur even in sophisticated models like Stable Video Diffusion (SVD) [70, 101]. Even top models like Sora [64] and Google's VideoPoet [102] show coherence issues or generate implausible scenarios [26]. A critical gap is the lack of explicit physical dynamics modeling and coherent scene understanding, leading to unrealistic motion and interactions [26]. Incorporating world models to learn physical principles and causality [95, 103] is a promising research direction. These could mitigate temporal inconsistencies by enforcing structured scene understanding and dynamic constraints [103, 104]. Motivated by these persistent limitations in achieving temporal and *physical* realism, our work proposes detection methods that exploit subtle irregularities in the geometric properties of neural representations [1, 2].

A.1 Qualitative Examples of Perceptual Trajectories

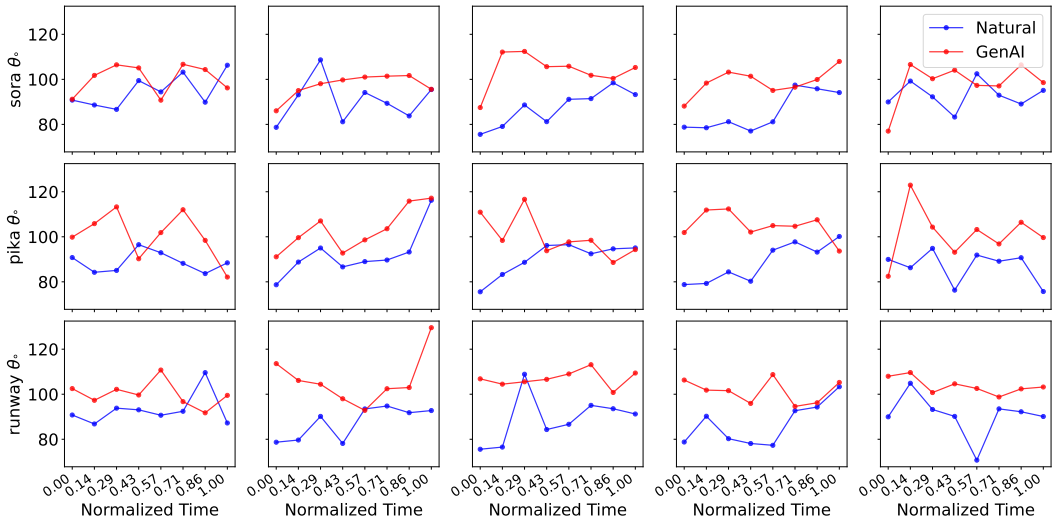

Figure 8: **Examples of raw curvature trajectories** (θ_i) over normalized time for pairs of natural videos (blue) and AI-generated videos (red) from different generative models (Sora, Pika, Runway). Each column represents a different example pair. These qualitative examples illustrate the tendency for AI-generated videos to exhibit different curvature patterns, with more erratic fluctuations compared to their natural counterparts when viewed in the DINOv2 representation space.

To provide a more intuitive understanding of how curvature trajectories differ, Figure 8 presents several qualitative examples. Each plot shows the sequence of calculated curvature values (θ_i) for a natural video (blue line) and a corresponding AI-generated video (red line) from the Sora [68], Pika [46], or Runway [81] models, after processing through the DINOv2 encoder as in Section 5.

While individual trajectories can be noisy, these examples visually highlight common tendencies observed: AI-generated videos frequently display trajectories with different overall levels of curvature, more pronounced peaks, or more erratic behavior compared to the often smoother or distinctly patterned trajectories of natural videos.

A.2 ReStraV Classifiers Results Analysis

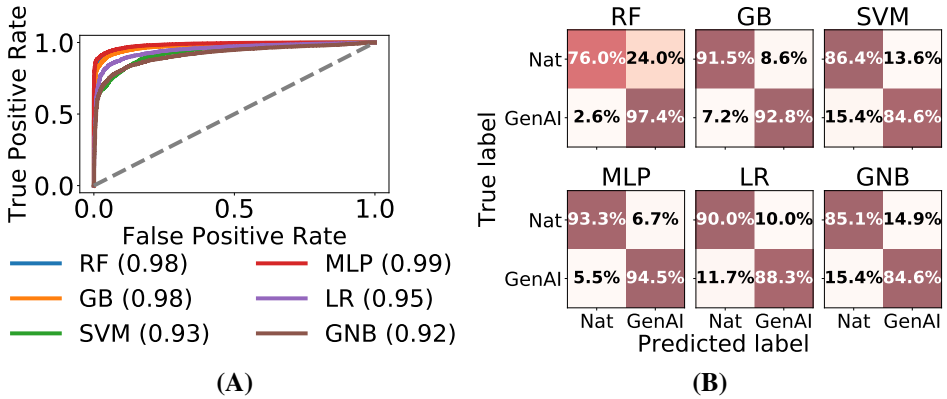

Figure 9: **(A) ROC curves** for various classifiers (Logistic Regression, Gaussian Naive Bayes, Random Forest, Gradient Boosting, SVM, MLP) on the test set. The MLP achieve the highest AUROC. **(B) Normalized confusion matrix for the ReStraV classifiers** on the test set, illustrating rates for both natural (Nat) and AI-generated (GenAI) classes. Values are percentages.

Figure 9A presents the ROC curves for all classifiers detailed in Table 1. The curve for the MLP (ReStraV) is closest to the top-left corner and with the largest area, AUROC (98.63%). Figure 9B displays the normalized confusion matrices for the *ReStraV* classifiers from Section 6. The strong diagonal elements (e.g., correctly identifying natural videos as "Nat" and AI-generated as "GenAI") and low off-diagonal values highlight the effectiveness. Specifically, correctly classifies a high percentage of both natural and AI-generated instances, aligning with the balanced accuracy and individual precision/recall/specificity metrics reported in Table 1.

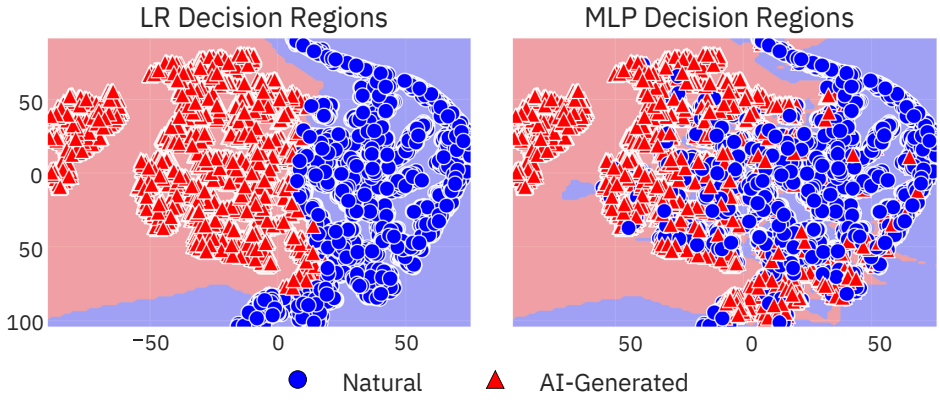

Figure 10: **Decision boundaries for Logistic Regression (LR) and Multi-Layer Perceptron (MLP) *ResTraV*'s classifiers.** The plots illustrate how these models partition a 2D projection of the feature space (detailed in Section 6) to distinguish between natural (blue circles) and AI-generated (red triangles) videos. This comparison highlights the different decision boundaries learned by a linear (LR) and a non-linear (MLP) model when applied to the geometric trajectory features.

For demonstration purpose, we construct Voronoi tessellations to visualize the decision boundaries obtained from two different classification models: Logistic Regression (LR) and a Multi Layer Preceptor (MLP) classifier from Section 6 in Fig. 10. The visualization underscores the benefit of

using a non-linear classifier for this task, given the nature of the feature space derived from *ReStraV*'s geometric analysis.

A.3 Feature Importance Analysis

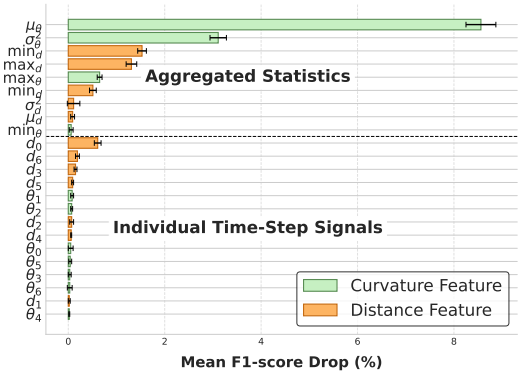

Figure 11: **Permutation Feature Importance.**The plot shows the mean drop in F1-score (%) when each feature is permuted, with error bars indicating standard deviation. Features are grouped into "Aggregated Statistics" (e.g., mean, variance) and "Individual Time-Step Signals" (e.g., d_0, θ_1). The results highlight the overwhelming importance of the mean curvature (μ_θ) and other aggregated statistics in distinguishing natural from AI-generated videos.

To identify which of the 21 features contributed most to the performance of our best classifier (the MLP), we conducted a permutation feature importance analysis. We trained the MLP on the 50,000 AI-generated and 50,000 natural videos described in Section 5 and then measured the drop in F1-score when each feature was individually shuffled. A larger drop indicates a more important feature. The results are visualized in Fig. 11.

The mean curvature (μ_θ) is unequivocally the most critical feature. Its importance is more than double that of the next most influential feature, the curvature variance (σ_θ^2). This provides strong quantitative evidence that the overall "straightness" of a trajectory is the primary signal our method leverages. The eight aggregated statistical features occupy the top tiers of importance. In contrast, the features representing individual, time-specific distance and curvature values (d_i, θ_i) have a much smaller impact, suggesting they provide complementary but less critical information. These findings validate the distributions shown in Figure 5, where the aggregated statistics for curvature and distance showed the clearest separation between natural and AI-generated videos. The classifier effectively learns to exploit these high-level geometric properties.

A.4 Qualitative Examples of "Plants" Task

Figure 12: **Sample from the GenVidBench "Plants" task** [17] for natural video (HD-VG/130M) and AI-generated plant video frames (MuseV [69], SVD [70], CogVideo [71], and Mora [72]).

Figure 12 shows qualitive samples of "Plants" task (P) [17]. This task involves videos where the primary subject matter is various types of flora. Natural videos (HD-VG/130M [100]) exhibit typical characteristics of real-world plant footage. The AI-generated examples from MuseV [69], SVD [70], CogVideo [71], and Mora [72] showcase the capabilities of these models in synthesizing plant-related content. While visually plausible, these AI-generated videos contain subtle temporal unnatural patterns (e.g., texture evolution) that *ReStraV* detect through its geometric trajectory analysis. The performance of ReStraV on this hard task are described in Table 4(P).

A.5 Results Distributions for Main Task (M) and Plants Task (P)

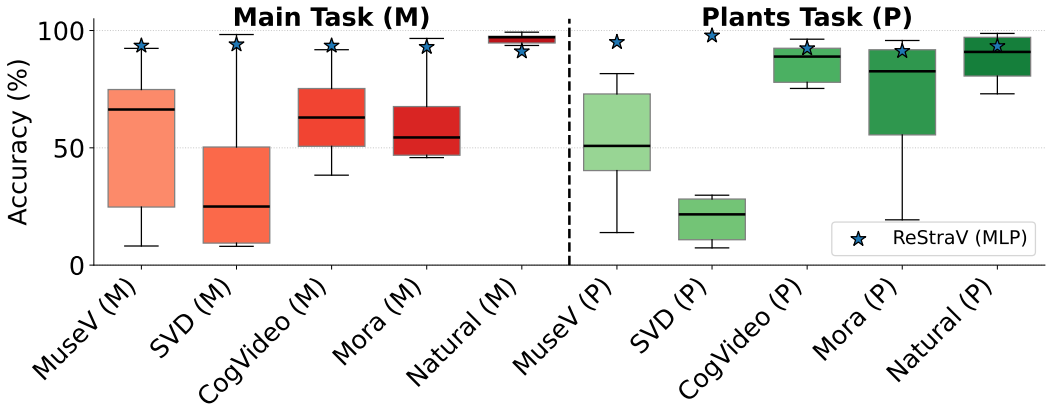

Figure 13: Accuracy distributions of *ReStraV* (MLP) and SoTA methods on GenVidBench [17]. Boxplots summarize performance on the Main task (red distributions) and Plants task (green distributions) across the different generative models within each task.

Figure 13 visualizes the accuracy distributions of various detectors, including *ReStraV* (MLP), on the GenVidBench Main (red distributions) and Plants (green distributions) tasks. The boxplots illustrate the median accuracy, interquartile range (IQR), and overall spread of performance for each method across the different generative models within each task. *ReStraV* (MLP) is consistently positioned at the higher end of the accuracy spectrum for both tasks, indicating more stable performance across different generators. For the Main task, ReStraV's median and overall distribution are visibly superior. For the Plants task, ReStraV again demonstrates leading performances. This visualization complements Table 4 by providing a overview of performance consistency and superiority.

A.6 Frame Samples from the Veo3 Model for Zero-shot Generalization Test

To provide a qualitative sense of the videos used in our zero-shot generalization test (Section 7, Paragraph D), Figure 14 presents sample frames generated by the Veo3 model. These examples illustrate the high quality of the content our method was tested against without any prior training on this specific generator.

B Ablation Studies

We performed ablation studies to understand the impact of key frame sampling parameters on the performance and efficiency of *ReStraV*. We randomly selected 10,000 AI-generated videos by Sora [68] from VidProM [3] and 10,000 natural videos from DVSC2023 [47]. The Sora [68] videos, with longer lengths (5s) and high frame rate (30 FPS as the natural videos), provide a robust basis for evaluating a wide range of sampling parameters, making them a good representative case for the AI-generated set. Performance is evaluated using Accuracy (%), AUROC (%), and F 1 Score (%), with inference time measured in milliseconds (ms). The shaded regions in the plots represent ±1 standard deviation around the mean, based on multiple runs involving different random video samples and 50/50 train-test partitioning. We use the best performer classifier (two-layer MLP $(64 \rightarrow 32)$) from Section 6 of the main paper.

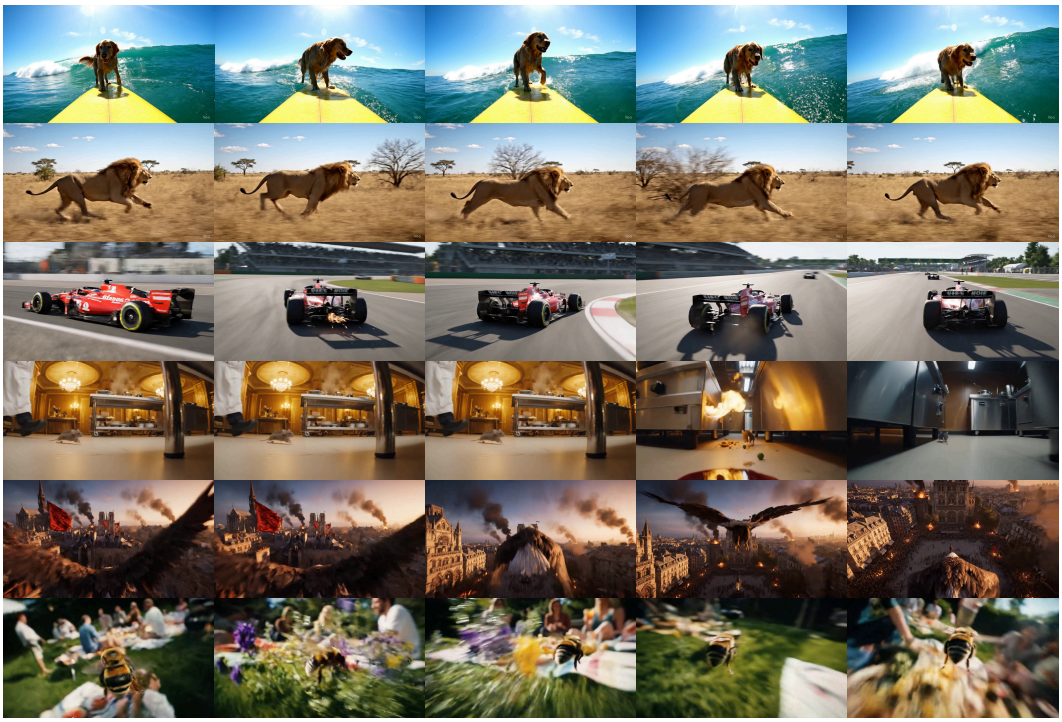

Figure 14: **Qualitative frame examples from the Veo3 [65] model.** These images showcase the high-fidelity content used for the zero-shot generalization test.

B.1 Impact of Video Length and Sampling Density

We investigated how the length of the video analyzed and the density of frame sampling within a fixed window affect *ReStraV*'s performance. The results are shown in Supplementary Figure 15.

Panel (a) of Supplementary Figure 15 illustrates the effect of varying the analyzed video length from 1 to 5 seconds, from which *ReStraV* processes a 2-second segment by sampling every 3rd frame (at 30 FPS). This results in the number of frames (T) input to DINOv2 [25] being 10, 20, 30, 40, and 50 for the respective conditions. As shown, performance metrics (Accuracy, AUROC, and F_1 score for AI-generated content) improve as the analyzed video length increases, with AUROC exceeding 96% for 2-second segments ($T \approx 20$) and reaching approximately 98% for 5-second segments ($T = 50$). Inference time increases linearly with T. The 2-second segment analysis, as used in our main paper (where $T = 24$ frames are processed), offers a strong balance between high performance and computational efficiency (observed around 40-48ms in related tests).

Panels (b) and (c) of Supplementary Figure 15 show the sampling density within a fixed 2-second source video (30 FPS, 60 total frames). Panel (b) shows performance against the sampling interval k (where every k^{th} frame is taken). The results indicate optimal performance when $k = 3$ ($T = 20$ frames), achieving an AUROC of $\approx 97\%$. Performance degrades for sparser sampling (e.g., $k = 5$, $T = 12$) and also for very dense sampling (e.g., $k = 1$, $T = 60$). Panel (c) plots performance directly against the number of sampled frames T, confirming peak performance at $T = 20$.

B.2 Robustness to Temporal Window Position

We also studied the impact of the starting position of the 2-second window when applied to 5s videos. A 2-second window (processed with *ReStraV*'s standard $T = 24$ frames) was slid across a 5-second video with a step of 10 frames (approximately 0.33s at 30 FPS).

As shown in Supplementary Figure 16, the detection performance remains largely robust regardless of the window's start time. A slight U-shaped trend is observed, with marginally higher performance at the beginning and end of the analyzed 0-3s window start time range, and a minor dip when the

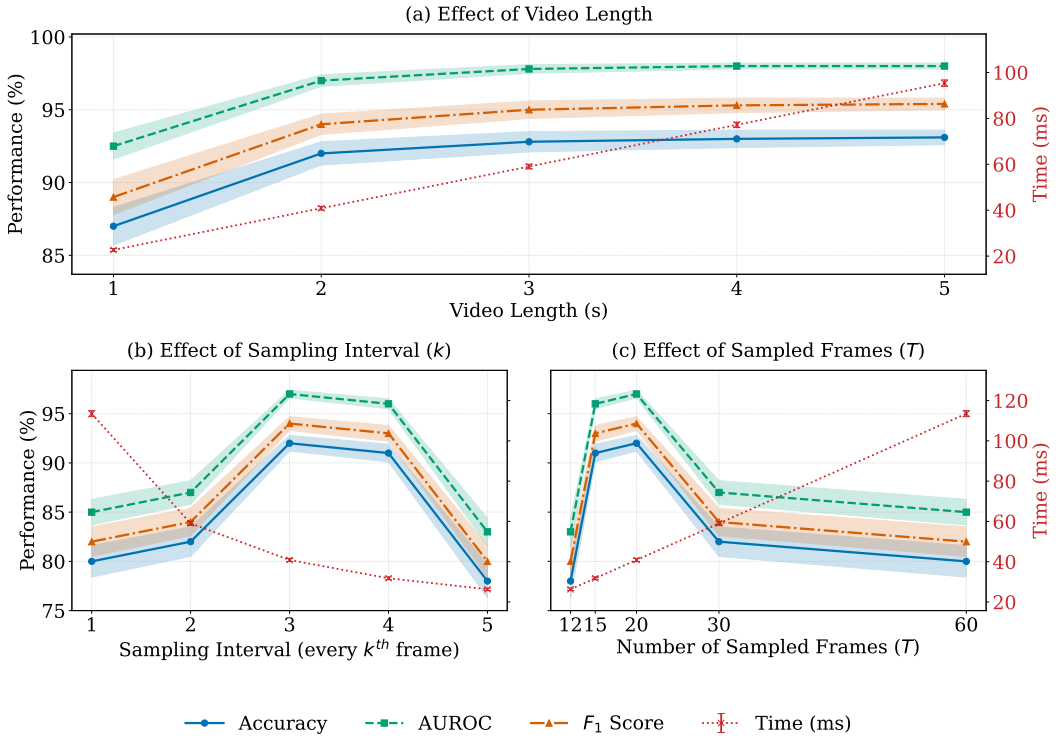

Figure 15: **Ablation on Video Length, Sampling Interval, and Number of Frames.** (a) Effect of analyzed video length. (b) Effect of sampling interval (k) for a 2s video. (c) Effect of total sampled frames (T) for a 2s video, derived from varying k.

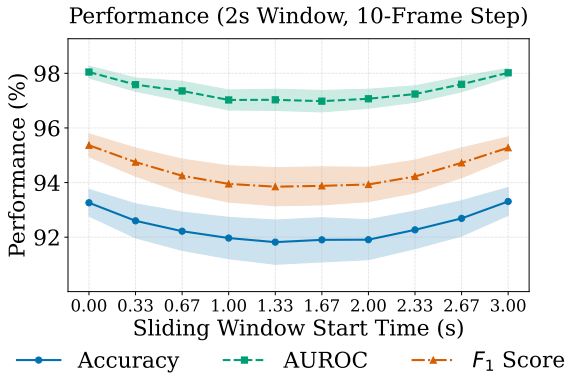

Figure 16: **Ablation Study on Sliding Window Start Time.** Performance of *ReStraV* when a 2s window (with $T = 24$ frames) slides across a 5s video with a 10-frame step.

window is centered. This demonstrates that ReStraV is not overly sensitive to the precise temporal segment analyzed within a longer video.

C Analysis of Scene Cut Frequency

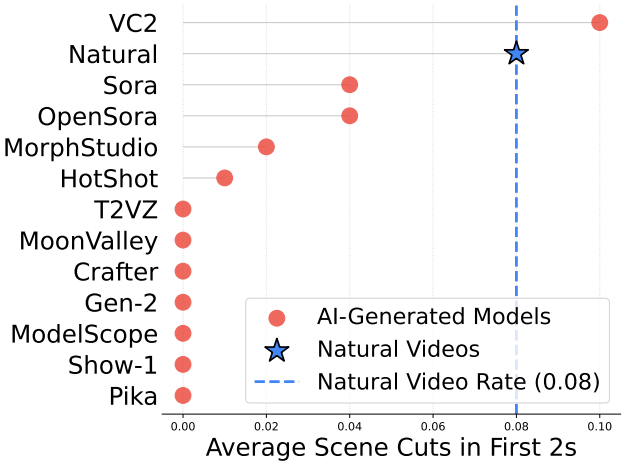

Model	Avg. Duration (s)	Avg. Cuts in first 2s
Pika	2.97	0.00
Show-1	3.62	0.00
ModelScope	3.84	0.00
Gen-2	4.00	0.00
HotShot	4.60	0.01
Crafter	5.43	0.00
MoonValley	5.59	0.00
T2VZ	6.01	0.00
VC2	6.98	0.10
Natural	**7.04**	**0.08**
MorphStudio	7.05	0.02
OpenSora	8.22	0.04
Sora	12.40	0.04

Figure 17: **Analysis of Scene Cut Frequency.** The lollipop plot (left) and table (right) show the average number of hard scene cuts within the first 2s for each video source. The dashed blue line in the plot indicates the rate for natural videos. Both visualizations confirm that the scene cut frequency is low across all models and not a significant confounding factor.

An important consideration for AI-generated video detection is the effect of hard scene cuts, as the straightening hypothesis is not expected to hold across shot boundaries. This presents a potential confound: if AI-generated videos simply contained a higher frequency of scene cuts, it could partly explain our classifier's performance.

To investigate this possibility, we analyzed 13,000 AI-generated and 13,000 natural videos using the "scenedetect" [105] library. The results, presented in Fig. 17, show that the average number of scene cuts is low and comparable for both natural and AI-generated videos. The plot (left) visualizes this comparison, showing all models clustering near the natural video baseline (dashed line), while the table (right) provides the precise data.

Our method's reliance on a short, 2s analysis window inherently reduces the probability of encountering a scene cut. The overall robustness of our approach is further confirmed by the ablation study in Section B.2, which shows stable detection performance regardless of the analysis window's temporal position.

D Computational Environment

All experiments presented in this paper were conducted on a system equipped with NVIDIA RTX-2080 GPUs, each with 8GB of VRAM. The feature extraction process using the DINOv2 ViT-S/14 model, which involves a forward pass for an 24-frame batch, takes approximately 43.6 milliseconds.

E Dataset Licenses and Sources

- **VidProM [3]:** This dataset was employed for training our video classifier (Section 6) and for benchmarking in Section 7 and Section 7. The VidProM dataset is offered for non-commercial research purposes under CC BY-NC 4.0 license.
- **GenVidBench [17]:** GenVidBench was used for benchmarking in Section 7). The GenVidBench dataset and its associated code are under CC BY-NC-SA 4.0 license.

- **Physics-IQ [26]:** This dataset facilitated the evaluation of our method on matched pairs of natural and AI-generated videos that depict physical interactions (Sec. 4, Sec. 7). The Physics-IQ dataset is available under the Apache License 2.0.
- **DVSC2023 (Natural Video Source for Classifier Training):** As explained in Section 5, a set of 50,000 natural videos for training (Section 6) was sourced from DVSC2023 [47]. DVSC2023 is under the CC BY-SA 4.0 llicense.